Numerical evidence for a chiral spin liquid in the XXZ antiferromagnetic Heisenberg model on the kagome lattice at m=2/3 magnetization

Krishna Kumar, Hitesh J. Changlani, Bryan K. Clark, and Eduardo Fradkin

Phys. Rev. B **94**, 134410 — Published 10 October 2016

DOI: 10.1103/PhysRevB.94.134410

Numerical evidence for a chiral spin liquid in the XXZ antiferromagnetic Heisenberg model on the kagome lattice at $m = \frac{2}{3}$ magnetization

Krishna Kumar, Hitesh J. Changlani, Bryan K. Clark, and Eduardo Fradkin
Department of Physics and Institute for Condensed Matter Theory,
University of Illinois at Urbana-Champaign, 1110 West Green Street, Urbana, Illinois 61801-3080
(Dated: August 22, 2016)

We perform an exact diagonalization study of the spin-$1/2$ XXZ Heisenberg antiferromagnet on the kagome lattice at finite magnetization $m = \frac{2}{3}$ with an emphasis on the XY point ($J_z = 0$), and in the presence of a small chiral term. Recent analytic work by Kumar, Sun and Fradkin [Phys. Rev. B 90, 174409 (2014)] on the same model, using a newly developed flux attachment transformation, predicts a plateau at this value of the magnetization described by a chiral spin liquid (CSL) with a spin Hall conductance of $\sigma_{xy} = \frac{1}{2}$. Such a state is topological in nature, has a ground state degeneracy and exhibits fractional excitations. We analyze the degeneracy structure in the low energy manifold, identify the candidate topological states and use them to compute the modular matrices and Chern numbers all of which strongly agree with expected theoretical behavior for the $\sigma_{xy} = \frac{1}{2}$ CSL. **In the limit of zero chirality, we find on most (not all) clusters that the topological invariants are still those of a CSL.**

I. INTRODUCTION

Quantum spin liquids have been the focus of a great deal of research for over two decades and are expected to exist in frustrated quantum antiferromagnets. A natural model, both theoretically and experimentally, to look for these states is the spin-$\frac{1}{2}$ quantum Heisenberg antiferromagnet on the kagome lattice. The discovery of materials such as Herbertsmithite, which do not appear to order down to the lowest accessible temperatures [1, 2] and, at least qualitatively, are described by this simple model, has given new impulse to theoretical investigations [3–10]. Relatively recent reviews on spin liquid phases in frustrated quantum antiferromagnets can be found in Refs. [11–13].

Several types of spin liquid states have been proposed to exist in quantum antiferromagnets [14] (of which the kagome lattice is a notable example), for example, topological states such as the time-reversal invariant $\mathbb{Z}_2$ spin liquid [15–17] (also known as the Toric Code state [18]) and the double-semion spin liquid [19], Dirac spin-liquid [7], as well as chiral spin liquid (CSL) [20]. In the absence of an external (Zeeman) magnetic field there is good evidence for a $\mathbb{Z}_2$ spin liquid being the ground state [3, 4], although other energetically competitive phases have also been reported [5, 7, 9]. On the other hand, a CSL has been found on addition of terms that explicitly break the chiral symmetry [21–26]. There is also evidence for the CSL phase in a Heisenberg antiferromagnet with further neighbor Ising interactions [27–29].

Most spin liquids have been discovered in zero external magnetic field, and here we explore the alternate possibility of finding one in finite field. We thus study the spin-$\frac{1}{2}$ quantum XXZ Heisenberg antiferromagnet on the kagome lattice (henceforth referred to as KAF) at finite magnetization. The Hamiltonian of the KAF is,

$$H_{XXZ} = \sum_{\langle i,j \rangle} J_{xy} \left(S_i^x S_j^x + S_i^y S_j^y \right) + J_z S_i^z S_j^z - h_B \sum_i S_i^z \tag{1.1}$$

where J_{xy} (set to 1 in this paper) and J_z are the strengths of the transverse and Ising terms respectively, and h_B is the external field. Indices i, j are used for sites, $\langle i, j \rangle$ refers to nearest neighbor pairs and $S^{x,y,z}$ refer to the usual spin-1/2 Pauli matrices. Since the Hamiltonian conserves total S_z, it is also common to simply drop the h_B term and instead work at fixed magnetization (m), defined as,

$$m \equiv \frac{n_\uparrow - n_\downarrow}{n_\uparrow + n_\downarrow} \tag{1.2}$$

where $n_\uparrow$ ($n_\downarrow$) are the number of up (down) spins.

Several facets of the model of Eq.(1.1) have been studied with different analytic and numerical techniques. For example, in the regime of strong Ising anisotropy, $J_z > J_{xy}$, a strong coupling expansion and exact diagonalization (ED) study has found evidence for valence-bond ordered phases at $m = 1/3$ magnetization [30]. At the Heisenberg point, $J_z = J_{xy}$, ED [31] and density-matrix renormalization group calculations [32] have found strong evidence for magnetization plateaus at $\frac{1}{3}$, $\frac{5}{9}$ and $\frac{7}{9}$ of the saturation value, and have further substantiated the existence of ordered phases.

While the Heisenberg and Ising regimes appear to have been systematically explored, less is known about the XY regime, i.e. close to $J_z = 0$. Analytic studies of the KAF in the XY regime using flux attachment methods predict magnetization plateaus at $\frac{1}{3}$ and $\frac{5}{9}$ magnetization (just like the Heisenberg case) in addition to one at $\frac{2}{3}$ magnetization, all of which correspond to CSL states [33]. These CSLs belong to the universality class of the Laughlin state for bosons with spin Hall conductance $\sigma_{xy} = \frac{1}{2}$ for the $m = \frac{1}{3}$ and $m = \frac{2}{3}$ plateaus, and the first Jain state for bosons with $\sigma_{xy} = \frac{2}{3}$ for the plateau at $m = \frac{5}{9}$ [33]. The CSL was postulated originally by Kalmeyer and Laughlin [34] as the ground state for the quantum antiferromagnetic spin-$\frac{1}{2}$ Heisenberg model on the triangular lattice. Note that the filling fraction of the corresponding fractional quantum Hall state is not equal to the filling fraction of the hard-core bosons (i.e. the magnetization fraction).

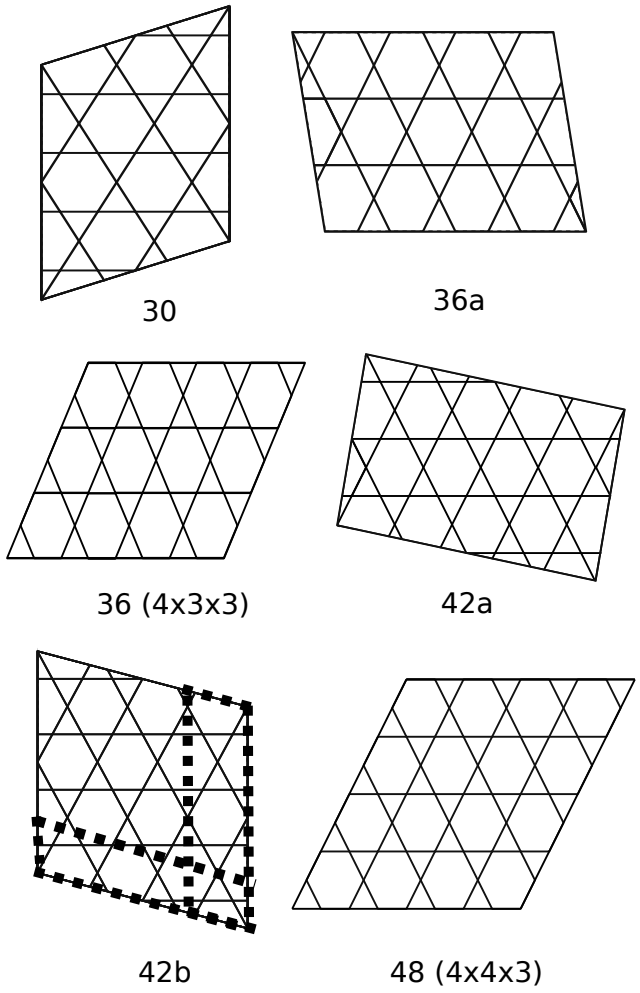

FIG. 1. Kagome clusters studied in the paper, notated in the standard way (see Ref. [10]). The case of 36d, not shown here, is presented in Appendix C. Dotted black lines on 42b site cluster correspond to two topologically non-trivial cuts used to compute the reduced density matrices and the corresponding MES states as outlined in Section V. Other clusters have similar cuts.

In this paper, we focus our attention to the case of the state with magnetization $m = 2/3$. This state is expected to be topological and described by an effective field theory with the form of a Chern-Simons gauge theory with gauge group $U(1)_k$ with level $k = 2$, which is the effective field theory of a fractional quantum Hall effect for bosons at filling fraction $\nu = \frac{1}{2}$. (For a detailed review see Refs. [35–37]). The CSL has the following properties: (a) it does not break any symmetries aside from time reversal and parity, (b) it has a two-fold degenerate ground state on a torus (i.e. a system with periodic boundary conditions), (c) its elementary excitations are anyons with fractional statistics $\theta = \frac{\pi}{2}$ (hence, they are semions) and fractional "charge" $\frac{1}{2}$, and (d) on a system with an open boundary it has a chiral edge state described by a chiral compactified $U(1)$ boson conformal field theory (CFT), also at level 2.

The topological properties of the CSL state on a torus are encoded in the modular $\mathcal{S}$ and $\mathcal{U}$ matrices which represent the response of the topological state to modular transformations of the torus [35]. In a general topological state, the matrix elements of the modular $\mathcal{S}$-matrix contain the quantum dimensions of the quasiparticles as well as their braiding properties, whereas the modular $\mathcal{U}$ matrix carries the information on the fractional spin, given in terms of the central charge of the associated chiral CFT and the conformal weight of the quasiparticles [38, 39]. In the case of the CSL (or the Laughlin state for bosons) there are two linearly independent states on the torus, represented by the identity state 1 and the Laughlin quasiparticle ψ_{qp}. The modular $\mathcal{S}$ and $\mathcal{U}$ matrices are given by the 2×2 matrices [40]

$$\mathcal{S} = \frac{1}{\sqrt{2}} \begin{pmatrix} 1 & 1 \\ 1 & -1 \end{pmatrix}, \qquad \mathcal{U} = e^{i\frac{2\pi}{24}1} \begin{pmatrix} 1 & 0 \\ 0 & i \end{pmatrix} \tag{1.3}$$

The factor of $\frac{1}{\sqrt{2}}$ in the $\mathcal{S}$ matrix is related to the effective total quantum dimension $D = \sqrt{2}$. [41] This also specifies the ground state degeneracy of such a state, which is two in this case. The phase of the $\mathcal{S}_{22}$ term can be related to the phase obtained by braiding two quasiparticles around one another. The value of -1 indicates that the effective quasiparticles are semions. The modular $\mathcal{U}$ matrix encodes the value of the central charge (which is $c = 1$ for a field theory expected to describe this phase) and the diagonal entries of the matrix give the phases that the various particles in such a system pick up under an exchange (for semionic quasiparticles it is $i = e^{i\frac{\pi}{2}}$). Hence, the modular matrices characterize the type of theory and the properties of the effective excitations or quasiparticles in the state.

Here we provide numerical evidence that the CSL is indeed realized in the KAF at $m = 2/3$. In order to aid the analysis, a small chiral term is added to the KAF Hamiltonian that allows us to probe a single chiral sector consisting of two topologically related states. We thus establish and verify analytical results that argued in favor of a CSL in the regime of XY anisotropy for $m = \frac{2}{3}$; amongst these is the result that the many-body Chern number and hence the spin Hall conductance is $\sigma_{xy} = \frac{1}{2}$ [33] and that the modular $\mathcal{S}$ and $\mathcal{U}$ matrices match those expected of a CSL.

The magnetization $m = \frac{2}{3}$ corresponds to a high total S_z sector, thereby restricting the Hilbert space and making the ED analysis feasible for reasonably large system sizes. To this end, we diagonalize the Hamiltonian of the KAF on finite clusters (discussed further in Section II) with up to 48 spins, with periodic boundary conditions. In Section III, we discuss the energy spectra as a function of model parameters and identify the quasi-degenerate ground states showing that these states are robust under flux pumping through the torus. Following this, in Section IV, we compute the many-body Chern number of the topological manifold finding it to be consistently 1/2 per state. In Section V, the topological states are used to determine the minimally entangled states along two different non-trivial topological cuts. This enables evaluation

of the modular matrices which are then compared to the predictions from topological field theory. All findings corroborate the existence of the CSL. We then consider in sec. VI and sec. VII the effects on the CSL as $J_\chi \to 0$ and $J_z > 0$ respectively. Finally, in Section VIII we conclude by summarizing our results.

II. CALCULATION DETAILS

As mentioned in the introduction, we focus our attention to the KAF Hamiltonian of Eq.(1.1) and implicitly choose h_B so as to fix the magnetization to $m = 2/3$. This problem is equivalent to considering a system of interacting hard-core bosons on the kagome lattice at 1/6 filling. In this mapping of spins to hard-core bosons, the term corresponding to J_{xy} is the kinetic energy and that corresponding to J_z is a density-density interaction. Notice that for the *antiferromagnetic* sign of J_{xy}, the kinetic energy describes bosons with a π flux on every triangle of the kagome lattice and, hence, it is frustrated. We focus primarily at the XY point, $J_z = 0$, where analytical work suggests the existence of a CSL [33].

While, the KAF is our primary interest, we have found it useful to consider the effects of adding a small chiral perturbation with strength J_χ. Thus the model we study is,

$$\begin{aligned} H_{total} =& H_{XXZ} + H_{chiral} \\ H_{chiral} =& J_\chi \sum_{\triangle} \vec{S}_i \cdot \left(\vec{S}_j \times \vec{S}_k \right) \end{aligned} \tag{2.1}$$

The chiral term is expected to naturally arise from the fermionic Hubbard model in a magnetic field and thus its inclusion is directly relevant to realistic materials. It must be kept in mind that the case of finite J_χ is not (in general) necessarily adiabatically connected to $J_\chi = 0$. For example, in the KAF at the Heisenberg point in zero field, a phase transition from a $\mathbb{Z}_2$ spin liquid to CSL occurs on the introduction of a fairly small chiral term [21].

Our motivation for working with finite J_χ is primarily to probe a single (rather than both) chiral sector, which allows us to cleanly separate the topological states from their chiral partners. This is needed since although the Zeeman term breaks time reversal symmetry, it does not break parity (i.e. mirror symmetry). Thus, a CSL state must break parity (chirality) spontaneously. The weak chiral term of Eq.(2.1) breaks the chiral symmetry explicitly. This greatly simplifies several analyses, especially when the energy scale corresponding to time reversal symmetry breaking is large (on the scale of the gap of the topological manifold to the rest of the spectrum) and all four states cannot be clearly identified. Further subtleties associated with this identification will be discussed in later sections.

We analyze the model of Eq.(2.1) using exact diagonalization of clusters of various sizes (ranging from 30 to 48 sites) and shapes, shown in Fig.1. Unless otherwise noted all clusters have periodic boundary conditions. Since there are several competing energy scales on the kagome lattice, the general extrapolation of properties to the thermodynamic limit is far from straightforward and each cluster requires individual consideration for detection of its topological manifold. In addition to the clusters shown in Fig. 1, we have performed calculations on cluster 36d, which we found to be similar to the 48 cluster, discussed further in Appendix C.

III. ENERGY SPECTRA AND GROUND STATE TOPOLOGICAL DEGENERACY

CSLs on a torus have topological degeneracy in the thermodynamic limit. A CSL with $\sigma_{xy} = \frac{1}{2}$ has two topologically degenerate states per chiral sector. By working at $J_\chi = 0.04$ (or $J_\chi = 0.05$), we explicitly (but weakly) break the time-reversal symmetry of the real valued XXZ Hamiltonian and therefore would expect to see two nearly degenerate states if the system is a CSL. This is substantiated from our results in Fig. 2 which shows the energy spectrum as a function of J_χ at the XY point ($J_z = 0.0$) for various clusters. On all clusters, for small values of $0.02 < J_\chi < 0.05$, we observe a clear two-fold quasi-degeneracy in the energy spectrum which is well separated in energy from the next lowest state for all clusters presented. (See Table I for the finite size energy gap to the closest and second-closest energy.) On most clusters, this feature persists even up to $J_\chi = 0$. For $J_\chi > 0.07$, the quasi-degeneracy ceases to exist suggesting the occurrence of a quantum phase transition. In addition, on the 48 site cluster, we see signs of a phase transition as a discontinuity in the first derivative of the ground state energy at $J_\chi = 0.053$.

For clusters 30, 36 and 36a and 42b the two quasi-degenerate states are in momentum sectors $K = (0,0)$ and $K = (\pi, 0)$ (or $K = (0, \pi)$) and for 42a they are in $K = (0,0)$ and $K = (\pi, \pi)$. For the rotationally symmetric 48-site cluster, the two low energy states lie in the $K = (0,0)$ momentum sector, consistent with the expectation that all the topological states are in $K = (0,0)$ when N_p/N_x and N_p/N_y are integers, where N_p is the number of particles and N_x and N_y are the number of unit cells in the x and y directions, respectively [42]. In 36d, presented in Appendix C, the two lowest states are also in $K = (0,0)$.

Topological states are expected to be locally indistinguishable. At $J_\chi = 0.04$, we compare the chiral expectation values around the three sites (labelled i, j, k) of a triangle Δ,

$$\chi_\Delta = \langle \vec{S}_i \cdot \left(\vec{S}_j \times \vec{S}_k \right) \rangle \tag{3.1}$$

of each of the two lowest states, finding that they are similar on all clusters with a value of approximately 0.06 (see Table I).

To probe the robustness of the proposed topological sector, we pump magnetic flux through non-trivial loops in the torus. Numerically, this is accomplished by twisting the boundary conditions resulting in the Hamiltonian $H(\theta_1, \theta_2)$ where the phase of $S_i^+ S_j^-$ terms are modified so as to preserve the translational symmetry of the lattice and ensure that any non-trivial

Clusters	Topological Gap	Excitation Gap	Chiral expectation	$\mathcal{S}$-matrix	Chern No. per state
30	0.000854	0.018358	$\langle\chi_{(0,0)}\rangle = 0.0684$ $\langle\chi_{(\pi,0)}\rangle = 0.0545$	$\begin{pmatrix} 0.697 & 0.701 \\ 0.717 & -0.713 \end{pmatrix}$	$\frac{1}{2}$ $\frac{1}{2}$
36a	0.000142	0.017929	$\langle\chi_{(0,0)}\rangle = 0.0676$ $\langle\chi_{(\pi,0)}\rangle = 0.0608$	$\begin{pmatrix} 0.706 & 0.708 \\ 0.708 & -0.706 \end{pmatrix}$	$\frac{1}{2}$ $\frac{1}{2}$
36	0.002186	0.020074	$\langle\chi_{(0,0)}\rangle = 0.0705$ $\langle\chi_{(0,\pi)}\rangle = 0.0554$	$\begin{pmatrix} 0.717 & 0.726 \\ 0.697 & -0.688 \end{pmatrix}$	$\frac{1}{2}$ $\frac{1}{2}$
36d	0.004890	0.016572	$\langle\chi_{(0,0)_1}\rangle = 0.0558$ $\langle\chi_{(0,0)_2}\rangle = 0.0537$	See Appendix C	1 ($\frac{1}{2}$ per state)
42a	0.0008262	0.022473	$\langle\chi_{(0,0)}\rangle = 0.0631$ $\langle\chi_{(\pi,\pi)}\rangle = 0.0622$	See Appendix A	0.510 0.490
42b	0.004374	0.025488	$\langle\chi_{(0,0)}\rangle = 0.0572$ $\langle\chi_{(\pi,0)}\rangle = 0.0546$	$\begin{pmatrix} 0.686 & 0.690 \\ 0.728 & -0.724 \end{pmatrix}$	$\frac{1}{2}$ $\frac{1}{2}$
48	0.006372	0.017958	$\langle\chi_{(0,0)_+}\rangle = 0.0531$ $\langle\chi_{(0,0)_-}\rangle = 0.0653$	$\begin{pmatrix} 0.705 & 0.694 \\ 0.694 & -0.736e^{-i0.088} \end{pmatrix}$	1 ($\frac{1}{2}$ per state)

TABLE I. Summary of results obtained on various clusters for $J_z = 0$ and $J_\chi = 0.04$. The chiral expectation values are computed on an elementary triangle of the kagome lattice and the sub-labels in the expectation correspond to the momentum (and rotation when applicable) eigenvalues of the candidate topological states. The modular matrices shown above are obtained using the same procedure described in the main text around Eq. (5.5) and (5.9).

loop around direction a of the lattice picks up total flux of θ_a.

As is shown in Fig. 3, we consider a 20×20 grid of (θ_1, θ_2) for the 42b and 48 clusters at $J_\chi = 0.05$ and plot the energy differences between the first three states in the two dimensional parameter space. The plot shows that the lower surface is clearly separated from the upper surface for all twists; this establishes the existence of a topological manifold that is gapped from the rest of the spectrum throughout the entire parameter space of flux pumps.

Fig. 3 also shows the spectral flow of the low energy states with respect to a twist angle; for the 42b (48) cluster the energy spectrum is plotted versus $\theta_2(\theta_1)$ at fixed $\theta_1 = 0$ ($\theta_2 = 0$). In the 42b case we observe that the $K = (0,0)$ and $K = (\pi, 0)$ momentum states flip exactly under the pumping of a 2π flux. This is characteristic of topological ground states; we will see in Sec. V that the individual ground states are minimally entangled states. Pumping a flux of 2π through a non-trivial loop on the torus allows for a transition from one topological sector to the other and the number of such 2π fluxes required for the system to return to its original state gives an indication of the ground state degeneracy. In this case we find two states consistent with a CSL.

Notice that in the case of the 48 site cluster, there is a third state that is not part of the topological manifold which is nonetheless separated from the rest of the continuum of low energy states. However, since it interlaces this manifold for small J_χ, it is suggestive of its possibly non-trivial role in the low energy physics.

Now that we have identified a topological manifold, we analyze our low energy wavefunctions in the next section and present evidence for the CSL state for small values of J_χ by computing the Chern number in the topological manifold and the field-theoretic modular matrices mentioned in the introduction.

IV. CHERN NUMBER

Given the separation of the ground state topological manifold from the continuum, it is meaningful to compute the combined Chern numbers of the two topological ground states. The Chern number, which is a topological invariant, is defined as the integral of the Berry curvature over the two dimensional

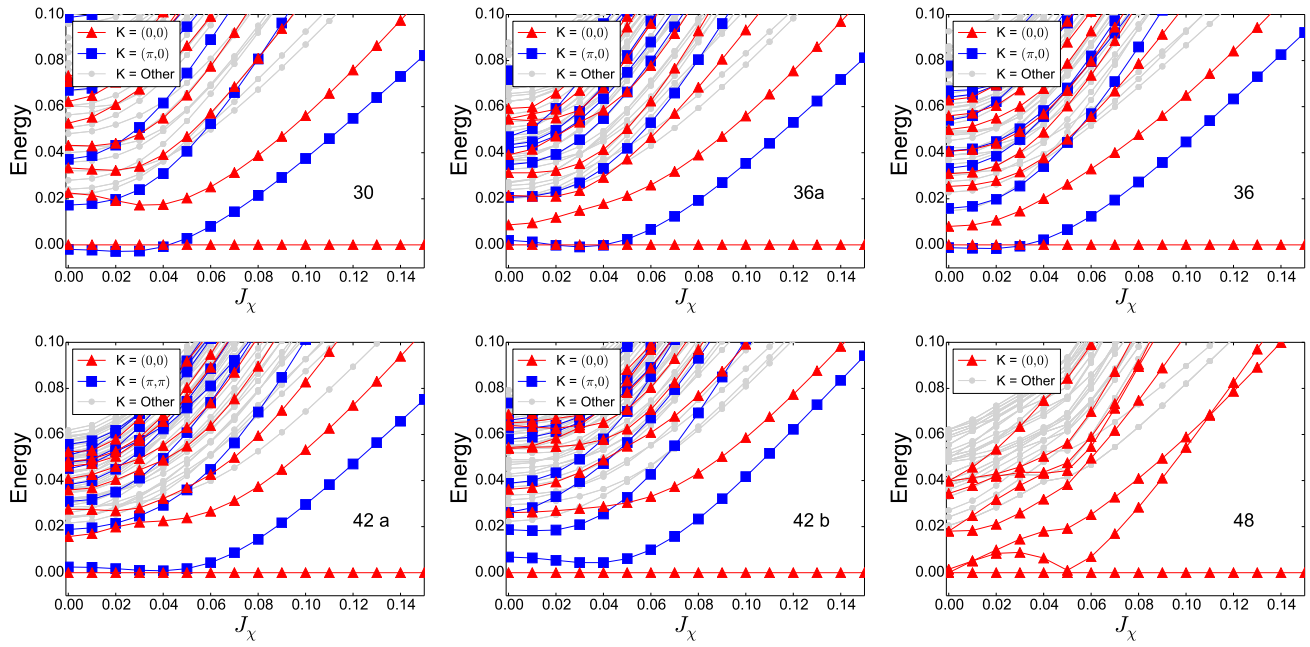

FIG. 2. Energy spectrum (relative to the ground state) as a function of J_χ at the XY point for clusters shown in Fig. 1. At finite but small J_χ a two fold degeneracy expected from the existence of a CSL is seen. On approaching $J_\chi = 0$, a four fold degeneracy is expected, but owing to finite size effects no clear separation of this manifold from the rest of the states is seen on any of the clusters.

zone of twist angles as,

$$C = \frac{1}{2\pi}\int_0^{2\pi}\int_0^{2\pi} B(\theta_1,\theta_2)d\theta_1 d\theta_2 \tag{4.1}$$

where $B(\theta_1,\theta_2)$ corresponds to the Berry curvature at the specific twist angles θ_1 and θ_2, which is defined as,

$$B(\theta_1,\theta_2) \equiv \partial_1 A_2 - \partial_2 A_1 \tag{4.2}$$

where $A_i(\theta_1,\theta_2)$ is the connection defined to be $A_i \equiv \langle\psi(\theta_1,\theta_2)|\partial_i|\psi(\theta_1,\theta_2)\rangle$.

Numerically, this calculation is carried out by first creating a grid of points in the (θ_1,θ_2) space where $\theta_1 \in (0,2\pi)$ and $\theta_2 \in (0,2\pi)$ (in practice, the largest grid chosen for such computations was 20×20). Then the eigenvector $|\psi(\theta_1,\theta_2)\rangle$ is computed, and the Berry curvature at each point is calculated as,

$$\begin{aligned} B(\theta_1,\theta_2) = \mathrm{Log}\{\ & \langle\psi(\theta_1,\theta_2)|\psi(\theta_1+\delta\theta_1,\theta_2)\rangle \\ & \times\langle\psi(\theta_1+\delta\theta_1,\theta_2)|\psi(\theta_1+\delta\theta_1,\theta_2+\delta\theta_2)\rangle \\ & \times\langle\psi(\theta_1+\delta\theta_1,\theta_2+\delta\theta_2)|\psi(\theta_1,\theta_2+\delta\theta_2)\rangle \\ & \times\langle\psi(\theta_1,\theta_2+\delta\theta_2)|\psi(\theta_1,\theta_2)\rangle\ \} \end{aligned} \tag{4.3}$$

which is essentially computing the overlap between wave functions along a closed loop in the (θ_1,θ_2) grid. The $\delta\theta_1$ and $\delta\theta_2$ in the above expression refer to the grid spacing along the θ_1 and θ_2.

When, the topologically related wavefunctions are in different momentum sectors they can be easily tracked individually and the gauge invariant quantity, i.e. the sum of the individual Chern numbers of the states can be computed directly by employing the formula above. When the two states cannot be (easily) tracked individually, such as the case on the 48 site cluster where both topological states are in the $K = (0,0)$ sector, a Non-Abelian formulation is used [43, 44], which yields $B(\theta_1,\theta_2)$ to be the log of a product of determinants.

The distribution of the Berry curvature, for $J_\chi = 0.05$, is shown in Fig. 4 as a function of θ_1 and θ_2 for the 42b and 48 site clusters. For the 42b case, individual contributions from each topological state using Eq. (4.1) and for the 48 site case the combined contribution of topological states from the Non-Abelian formalism, are shown. The Chern number for the $K = (0,0)$ and $K = (\pi,0)$ states of the 42b cluster are 0.5 and 0.5 and the combined value of the two $K = (0,0)$ states of the 48 cluster is 1, at least to 6 decimal places. Chern numbers for all cases studied are summarized in Table I.

We clarify that while the Chern number contributions from individual states can vary with J_χ, their sum is a gauge invariant quantity which is constant as long as the states remain topological. For example, at $J_\chi = 0.05$, the Chern numbers of the $K = (0,0)$ and $K = (\pi,\pi)$ states of the 42a cluster are 0.507 and 0.493, and 0.55 and 0.45 at $J_\chi = 0.025$. However, in all cases, for small J_χ, we find the same Chern number of $\frac{1}{2}$ per state. This is exactly the Chern number expected of a $\sigma_{xy} = \frac{1}{2}$ CSL.

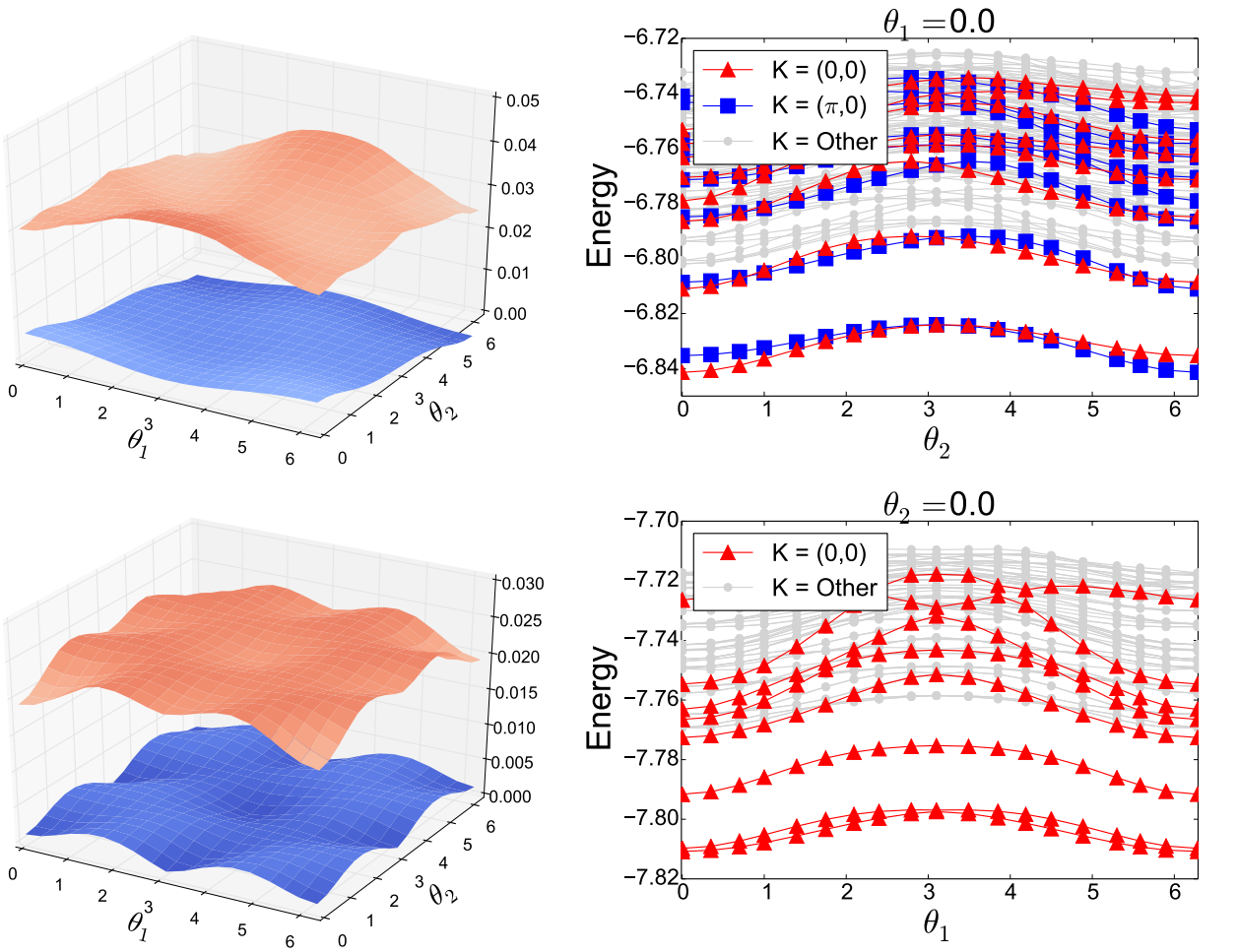

FIG. 3. Top: Energy differences of the 42b cluster for $J_\chi = 0.05$ and $J_z = 0$ of the first three states with respect to the state at $K = (0, 0)$ along the two twist directions (θ_1, θ_2) (left) and a representative cross section of the low energy spectrum along θ_2 at $\theta_1 = 0$ (right). The lowest $K = (0, 0)$ state and $K = (\pi, 0)$ states flip under flux pumping which is characteristic for degenerate states in different topological sectors. Bottom: Energy difference of the 48 cluster for $J_\chi = 0.05$ and $J_z = 0$ of the first three states with respect to the lowest energy state in $K = (0, 0)$ along the two twist directions (θ_1, θ_2) (left) and a representative cross section of the low energy spectrum along θ_1 at $\theta_2 = 0$ (right).

V. MINIMALLY ENTANGLED STATES AND MODULAR MATRICES

In this section we focus on the XY point in the presence of a small chiral term, specifically the results we present are for $J_\chi = 0.04$. On all clusters we use the lowest two quasi-degenerate states to compute the modular matrices following approaches used in Refs. [45–48]. In this scheme, minimally entangled states (MES) are determined from the low-energy exact wavefunctions along topologically non-trivial cuts (see for example cluster 42b on Fig.1) and then appropriate wavefunction overlaps between these MESs are evaluated.

We begin our analyses by considering the 48 site cluster where all the low-energy states belong to the $K = (0, 0)$ momentum sector. The 48 site cluster is symmetric under a rotation of $\pi/3$ and thus we label the lowest two states ($|\psi_+\rangle$ and $|\psi_-\rangle$) by their rotational eigenvalues, found to be, $\lambda_+ = \exp(i2\pi/3)$ and $\lambda_- = \exp(-i2\pi/3)$. To compute the MES, we first construct the generic normalized linear combination of the two topological states,

$$|\Psi\rangle = c\,|\psi_+\rangle + \sqrt{1-c^2}e^{i\phi}\,|\psi_-\rangle \tag{5.1}$$

where $c \in [0, 1]$ and $\phi \in (-\pi, \pi]$ are real parameters. Next, we consider two non-trivial partitions (i.e. two distinct non-contractible Wilson loops) on the torus and obtain the second Rényi entanglement entropy S_2 from the reduced density matrices as follows

$$\rho_I \equiv \mathrm{tr}_{I'}\,|\Psi\rangle\langle\Psi| \tag{5.2}$$

$$S_2 \equiv -\ln \mathrm{tr}\rho_I^2 \tag{5.3}$$

where ρ_I is the reduced density matrix for one of the cuts which we label as region I and the trace $\mathrm{tr}_{I'}$ runs over all the sites in region I' (I' corresponds to those sites that do

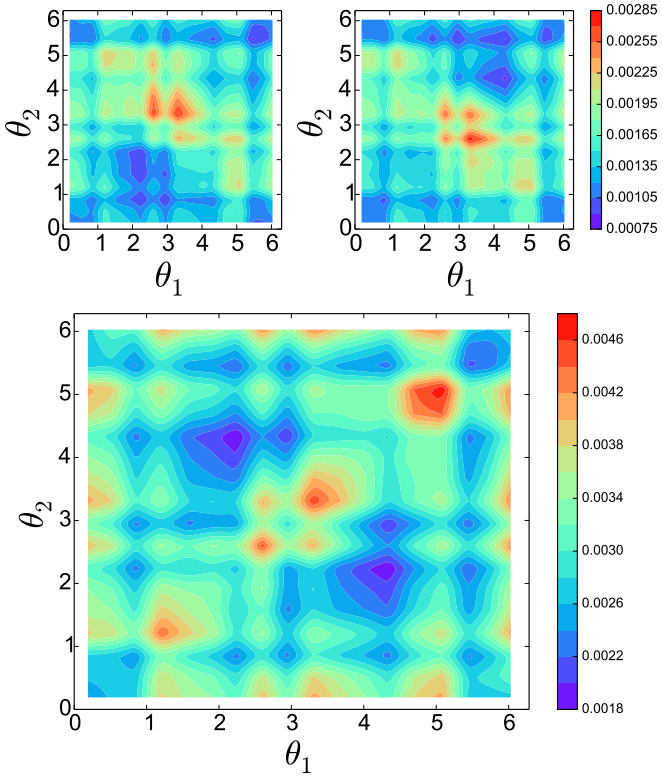

FIG. 4. Distribution of Berry curvature for the 42b $K = (0, 0)$ (top left) and $K = (\pi, 0)$ (top right) ground states and the two lowest $K = (0, 0)$ states of the 48 site cluster (calculated together in a Non Abelian formalism), at $J_z = 0$ and $J_\chi = 0.05$. For all clusters, the Chern number sums to $+1$.

not belong to the cut I). The MES states then correspond to local minima in the Rényi entanglement entropy in the (c, ϕ) parameter space.

For the 48 site cluster, the entanglement entropy as a function of (c, ϕ) is shown in Fig 5 for $J_z = 0.0$ and $J_\chi = 0.04$ along one non-trivial cut. We observe that there are indeed two local minima corresponding to,

$$\begin{aligned} |\Psi^1\rangle &= 0.462\,|\psi_+\rangle + 0.887 e^{i1.740}\,|\psi_-\rangle \\ |\Psi^2\rangle &= 0.901\,|\psi_+\rangle + 0.434 e^{i4.882}\,|\psi_-\rangle \end{aligned} \tag{5.4}$$

The overlap between the above two states is $\langle\Psi^1|\Psi^2\rangle \approx 0.0315$, the small deviation from orthogonality being a finite size effect. **The corresponding values of the entropy for the two minima are similar, in this case** 4.06 **and** 4.35**, the small difference possibly arising out of sub-leading corrections. (Note that the cuts comprised only of 12 sites, for which the area law of the entanglement entropy could have significant additional corrections).**

Due the rotational symmetry of the 48 site cluster, one can obtain the MES states along the other cut by applying the rotation operator by $2\pi/3$ on the above MES states. This symmetry is special and allows us to compute both the modular $\mathcal{S}$ and $\mathcal{U}$ matrices, for which we follow the procedure outlined in other numerical works [48] to carry out the calculation. Our result is,

$$\mathcal{S} = \begin{pmatrix} 0.705 & 0.694 \\ 0.694 & -0.736 e^{-i0.088} \end{pmatrix} \tag{5.5}$$

and

$$\mathcal{U} = e^{i\frac{2\pi}{24}1.014} \begin{pmatrix} 1.000 & 0.000 \\ 0.000 & i e^{0.053 i} \end{pmatrix} \tag{5.6}$$

The above modular matrices are in excellent agreement with the expected theoretical modular matrices shown in Eq. (1.3). We find similar modular matrices for $0.02 \lesssim J_\chi \lesssim 0.07$ on the 48 site cluster; above which there appears to be a single ground state with a large gap to the excited states. Further, this gap tends to grow rapidly for larger values of J_χ as can be seen in Fig. 2.

A similar behavior is also observed for other clusters (30, 36, and 42b) for values of $J_\chi \lesssim 0.07$; **the results for** $J_\chi = 0.04$ **are summarized in Table I.** On these clusters the topological ground states belong to different momentum sectors. (Since these clusters lack rotational symmetry, we are restricted to only computing the modular $\mathcal{S}$ matrix.) For example, for the 42b site cluster when $J_\chi = 0.04$, the lowest two energy states are in momenta sectors $K = (0, 0)$ and $K = (\pi, 0)$. respectively. Using these two topological states we get the below MES states along the two non-trivial cuts shown in Fig. 5. Along Cut I, we get

$$\begin{aligned} |\Psi_{I,1}\rangle &= 0.686\,|\psi_{(0,0)}\rangle + 0.728 e^{i2.639}\,|\psi_{(\pi,0)}\rangle \\ |\Psi_{I,2}\rangle &= 0.690\,|\psi_{(0,0)}\rangle + 0.724 e^{i5.781}\,|\psi_{(\pi,0)}\rangle \end{aligned} \tag{5.7}$$

and the overlap between these two states along Cut I is ≈ -0.0533. Along Cut II we get

$$\begin{aligned} |\Psi_{II,1}\rangle &= |\psi_{(0,0)}\rangle \\ |\Psi_{II,2}\rangle &= |\psi_{(\pi,0)}\rangle \end{aligned} \tag{5.8}$$

which gives the $\mathcal{S}$ matrix

$$\mathcal{S} = \begin{pmatrix} 0.686 & 0.690 \\ 0.728 & -0.724 \end{pmatrix} \tag{5.9}$$

The case of 42a is similar to the above clusters in that the topological states exist in different momentum sectors. While the MESs along one cut are found to be in agreement with the theoretical expectation, the profile of the entanglement (as a function of c, ϕ) along the other cut appears fairly flat, with only small variations in S_2 of the order of 0.1. This makes the identification of the MES and hence the evaluation of the $\mathcal{S}$ matrix unreliable. This is attributed to a finite size effect of the relevant topologically non trivial loop and discussed further in Appendix A.

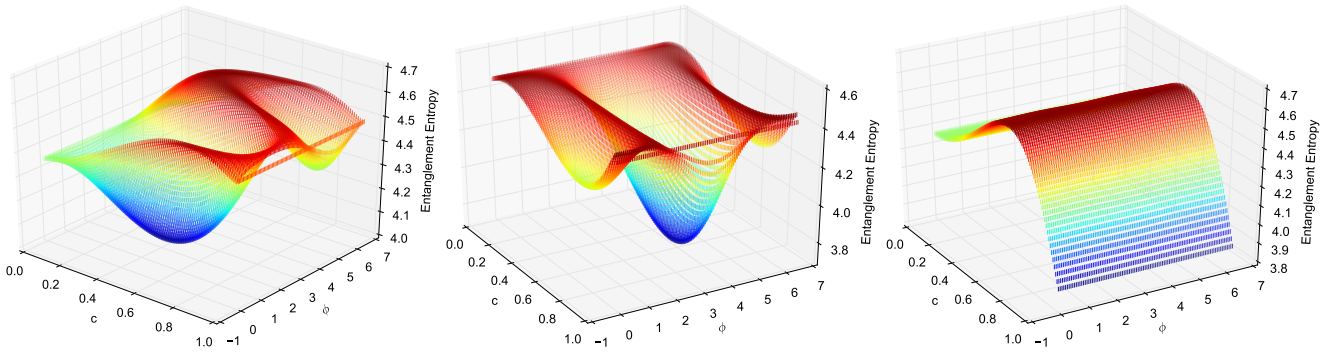

FIG. 5. Renyi entanglement entropy along topologically non trivial cuts as a function of c, ϕ for some representative cases. The entanglement for the 48 site cluster for $J_\chi = 0.04$ and $J_z = 0$ (left) shows two minima (the other cut is related by rotational symmetry). For the 42b cluster (for $J_\chi = 0$ and $J_z = 0$) two minima are also seen for both cuts (center) along the vertical and (right) horizontal directions. (see Fig. 1 for cut descriptions). Note that in the latter case the minima coincide with eigenstates and occur at the boundaries of the two dimensional parameter space.

VI. CASE OF $J_\chi \to 0$

In the previous sections, we have presented strong numerical evidence for the existence of a CSL phase in the $m = 2/3$ sector with a small $J_\chi \approx 0.04$ chiral symmetry breaking term. In this section, we consider the limit where $J_\chi \to 0$.

In this limit, our Hamiltonian is real and so (non-degenerate) states with non-zero chiral order must be spontaneously broken. This is true even though the introduction of a magnetic field has explicitly broken time-reversal symmetry in the spin language (there are more "up" than "down" spins); there is an additional time-reversal symmetry which is most evidently manifest in the bosonic language where the symmetry corresponds to the operation of charge conjugation of the bosons. Therefore, we anticipate four degenerate states in the thermodynamic limit: two topological states in each chiral sector. Unfortunately, as seen in Fig. 2, we do not observe four states clearly separated from the continuum in any cluster. Therefore, either the finite-size breaking of the two chiral sectors is large for these system sizes or the CSL does not survive in this limit.

Most Clusters: To explore this further, we first note that in all but the 48 and 36d cluster (i.e. 30, 36a, 36, 42a, 42b) , the two nearly degenerate states stay gapped out from the rest of the spectrum as $J_\chi \to 0$ suggesting the possibility that the finite-size breaking of the topological gap stays small while the chiral symmetry breaking gap is large. As noted earlier, the Chern numbers on the 42a and 42b clusters still are 1/2 per state at the lowest non-zero $J_\chi = 0.025$ that we explored. In the 42b case, at $J_\chi = 0$, we find that the all the contribution from the two-dimensional twist space to the Berry phase is found to arise from a single "Berry monopole", a single point carrying all the Chern number. This has a direct analog in the non-interacting band theory of topological insulators and is further discussed in Appendix B. The Chern number we compute in this situation is $\pm 1/2$ per state (the sign cannot be resolved because of the "Berry monopole."). Therefore, the Chern number for each state is still likely $1/2$ per state, although strictly speaking we cannot determine whether the gauge invariant sum of the two topological states is zero or one.

We compute the MES on the two lowest states, getting, in the case of the 42b cluster,

$$\mathcal{S} = \begin{pmatrix} 0.700 & 0.74 \\ 0.714 & -0.673 \end{pmatrix} \tag{6.1}$$

Once again, the above modular $\mathcal{S}$ matrix is in close agreement with the theoretically expected modular matrix consistent with the prediction that in the XY limit the ground state at $m = \frac{2}{3}$ is a CSL with semionic quasiparticle excitations.

We clarify that since these states are real and have no chiral expectation, the ideal scenario would be to identify the linear combination of states which form the chiral states and compute the MES on those. However, we find that these are located higher in the spectrum (and presumably mixed with other states), we do not attempt to make a definitive identification here.

The 48 site cluster: The 48 site cluster is more subtle as at $J_\chi = 0$, we observe not only two exactly degenerate states but also a third state only slightly higher in energy. The two exactly degenerate ground states are labelled as $|\psi_\pm\rangle$ and the third state as $|\psi_0\rangle$ state due to their eigenvalues under the $\pi/3$ degree lattice-rotation operator i.e. $R_{\frac{\pi}{3}} |\psi_\pm\rangle = \lambda_\pm |\psi_\pm\rangle$ and $R_{\frac{\pi}{3}} |\psi_0\rangle = \lambda_0 |\psi_0\rangle$ where $\lambda_\pm = e^{\pm i \frac{2\pi}{3}}$ and $\lambda_0 = 1$. As expected of a real valued Hamiltonian, the two exactly ground degenerate states are complex conjugates of one another i.e. $|\psi_+\rangle = |\psi_-\rangle^*$; their chiralities are found to be approximately $+0.008$ ($|\psi_+\rangle$) and -0.008 ($|\psi_-\rangle$).

We find under twisting of the boundary conditions that the third nearly degenerate state does interlace with the other two low-energy states (among other states). Therefore we cannot cleanly identify a low-energy topological sector for which we can compute Chern numbers or MES. On this cluster, we therefore need a large enough value of J_χ before we can confidently compute the topological properties.

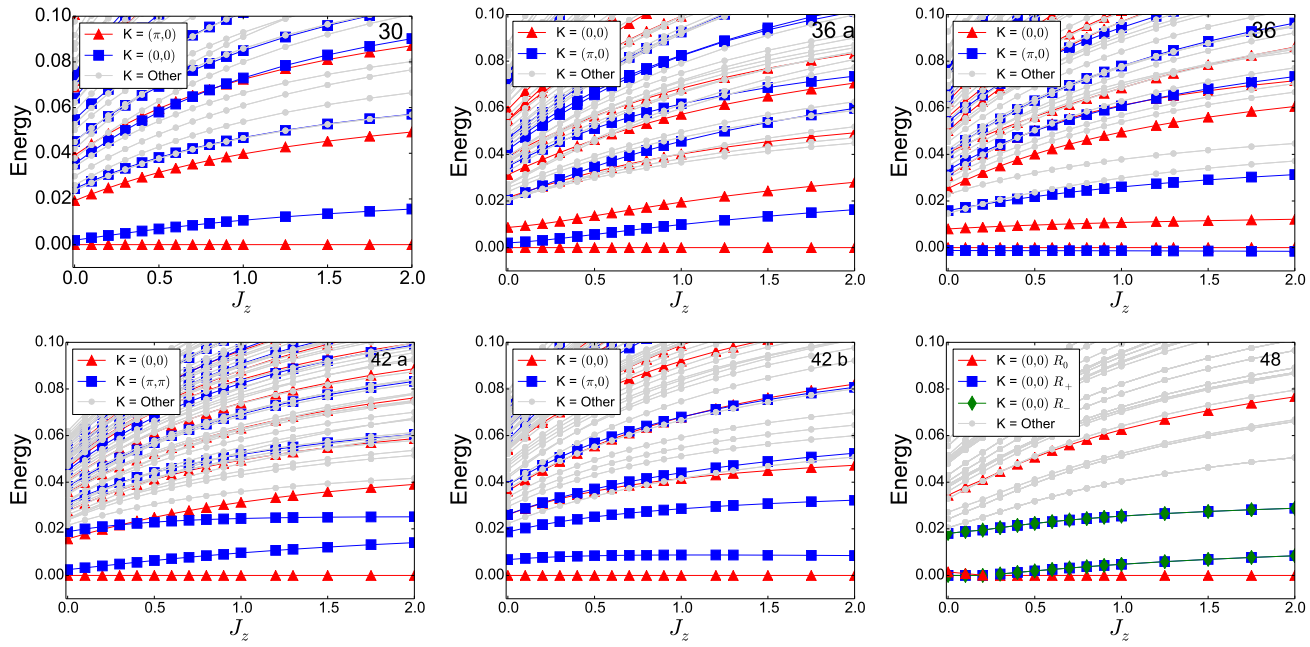

FIG. 6. Energy spectrum (relative to the ground state) as a function of J_z at $J_\chi = 0$ for clusters shown in Fig. 1. For most clusters (except the 48 site one), the low energy spectrum appears adiabatically connected to the large J_z limit.

VII. AWAY FROM THE XY POINT: $J_z > 0$

While we have primarily focused on $J_z = 0$, we will now consider the situation for $J_z > 0$ and $J_\chi = 0$. We show the spectrum as a function of J_z in Fig. 6. For the non-48 site clusters, there is no indication of a gap closing at any value of J_z out to $J_z \sim 2$ suggesting an adiabatic connection to the Ising limit. For 42b we computed both the Chern number and MES throughout this entire range of J_z and continue to find $C = 1/2$ per state and two local MES whose $\mathcal{S}$ matrix matches the predicted CSL one when taking the two lowest states. The exception to this observation is the 48 site cluster where there is a clear energy crossing at $J_z \approx 0.2$ with the $|\psi_0\rangle$ becoming the ground state. Given our current accessible system sizes, we are not able to arbitrate the true ground state phase at large J_z given this disagreement.

VIII. CONCLUSIONS

In summary, using exact diagonalization, we have analyzed the low energy properties of the XXZ antiferromagnetic Heisenberg model on the kagome lattice at $m = \frac{2}{3}$ magnetization with an emphasis on the XY regime and in the presence of a small chiral perturbation. We were able to identify the topological states in the ground state manifold on multiple clusters and showed that they have the expected characteristics of the chiral spin liquid predicted by analytical calculations [33]. We presented evidence of the chiral spin liquid with $\sigma_{xy} = \frac{1}{2}$ based on modular matrix computations which show the existence of semionic quasiparticles in these systems. We have also shown that flux pumping the states in different topological sectors evolve into one another as expected and finally also verified that the Chern numbers of the topological states are equal to $+1/2$.

All of the above calculations provide strong evidence for the existence of the topological state in the presence of a small chirality term. While we do not see the expected four degenerate states at $J_\chi = 0$ (possibly because of finite size effects), the topological invariants indicate, in this limit, a CSL on most clusters although some clusters show an additional competitive low-energy state. This suggests that either the chiral state may survive down to $J_\chi = 0$ or alternatively, the presence of a phase transition at very small $J_\chi \lesssim 0.02$.

IX. ACKNOWLEDGEMENT

We thank H. Shapourian and V. Chua for illuminating discussions, especially regarding the subtleties of flux pumping and evaluation of the many-body Chern number. HJC and BKC were supported by SciDAC-DOE grant DE-FG02-12ER46875. This work was supported in part by the National Science Foundation grant No. DMR 1408713 (K.K. and E. F.) at the University of Illinois. This research is part of the Blue Waters sustained petascale computing project, which is supported by the National Science Foundation (awards OCI-0725070 and ACI-1238993) and the State of Illinois. Blue Waters is a joint effort of the University of Illinois at Urbana Champaign and its National Center for Supercomputing Applications.

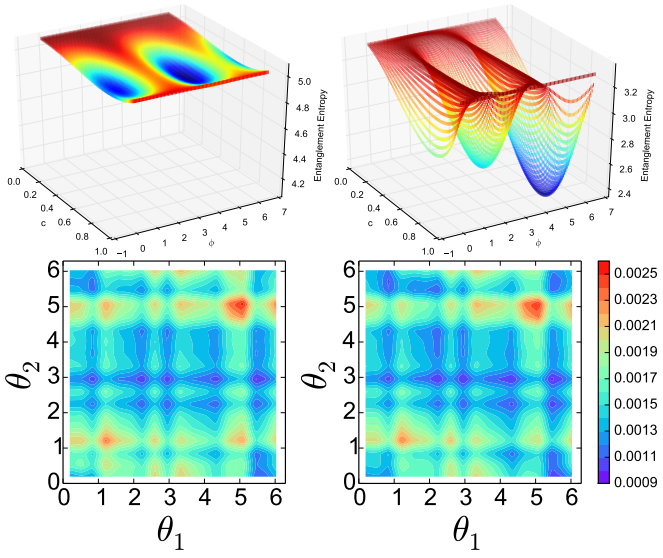

FIG. 7. Top: Renyi entanglement entropy for the 42a cluster obtained from the reduced density matrix along two topologically non-trivial cuts. Along the first cut (left), the entanglement entropy is found not to vary significantly. The locations of the minima along the second cut (right) are in agreement with the theoretical expectation. Bottom: Distribution of Berry curvature for the for the topological states in $K = (0, 0)$ (left) and $K = (\pi, \pi)$ (right); The Chern number over both states is computed to be 1.

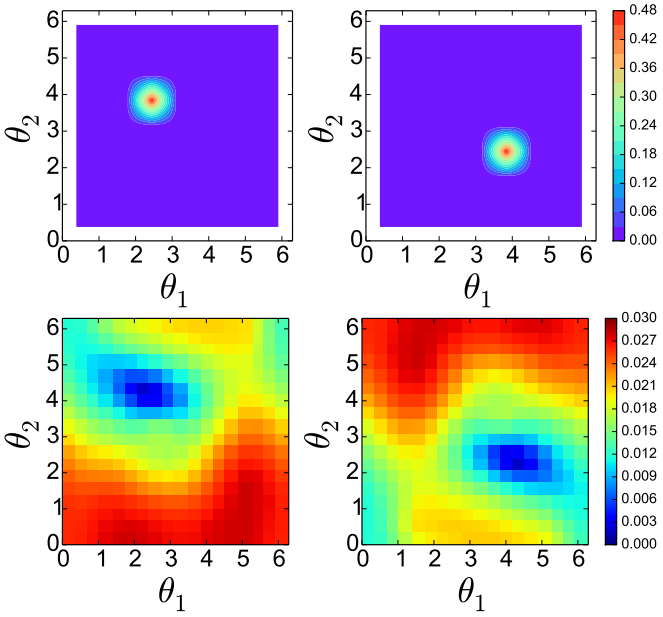

FIG. 8. Top: Berry curvature as a function of θ_1 and θ_2 for the ground states in $K = (0, 0)$ (left) and $K = (\pi, 0)$ (right) sectors in the case of time reversal symmetric Hamiltonian $J_\chi = 0$ on the 42b cluster. In both cases, there is essentially one point (marked by the bright red spot) on the entire grid that contributes to the total Chern number; the finite spread seen is an artefact of grid resolution and the interpolation used to present the distribution. Bottom: The energy difference between the first two states in each momentum sector. The point of touching of the two energy levels coincides with the location of high Berry curvature confirming it to be the source of the non-zero Chern number.

Appendix A: Modular matrices for the 42a case

In section V we discussed the case of the 42a cluster which naively did not yield orthogonal minimally entangled states (MES) along one of its cuts. On probing the Renyi entanglement entropy S_2 of this cut as a function of parameters specifying the MES, shown in Fig. 7, we observed that the profile appears fairly flat with no clear minima; the difference between the maxima and minima of S_2 is ≈ 0.1. This makes the identification of the MES and hence the evaluation of the $\mathcal{S}$ matrix unreliable. This may be due to the small width of the region (topologically non-trivial cut) used to compute the reduced density matrices. Note however that along the other cut, the minima of S_2 are prominent, and yield (nearly) orthogonal states, consistent with the theoretical expectation.

Fig. 7 also shows the distribution of the Berry curvature at $J_\chi = 0.05$ and $J_z = 0$, in the two dimensional twist space, for each of the topological states in momentum $K = (0, 0)$ and $K = (\pi, \pi)$. The Chern number (i.e. the integrated Berry curvature), summed over the two topological states is found to be 1 consistent with the expectation of a CSL.

Appendix B: Distribution of Chern number at $J_\chi = 0$

Consider a non-interacting band theory, where two bands touch at some point in momentum space, and assume this touching is protected by time-reversal. When a chiral term (time reversal symmetry breaking term) is added the bands do not touch any more, a gap at the special point is introduced and each band individually acquires a Chern number. Thus, in some sense the source of non-zero Chern number can be attributed to be emerging from the band touching in a time reversal symmetric model.

As explained in the text, with zero external chirality, the XXZ Hamiltonian is time reversal symmetric. The analogous observation in the case of many-body wavefunctions is that the source of non-zero Chern number is the ground and first excited state wavefunctions in the same momentum sector touching at one (or more) points in the two-dimensional space of twist angles. As is seen in Fig. 8 for the 42b cluster, we find a Berry monopole (a singular region which has non zero Berry curvature) when the lowest state in $K = (0, 0)$ or $K = (\pi, 0)$ is tracked; its location coincides with that of the twist at which the energy gap (in the corresponding momentum sector) goes to zero.

Note however, the phase assignment of the Berry monopole for the wavefunctions is ambiguous up to a sign ($\pm\pi$) in the absence of time-reversal symmetry. With the inclusion of the chiral term the time-reversal is broken, the Berry monopole spreads out (as is seen in Fig. 4 in the main text) and the sign of the Chern number is determined.

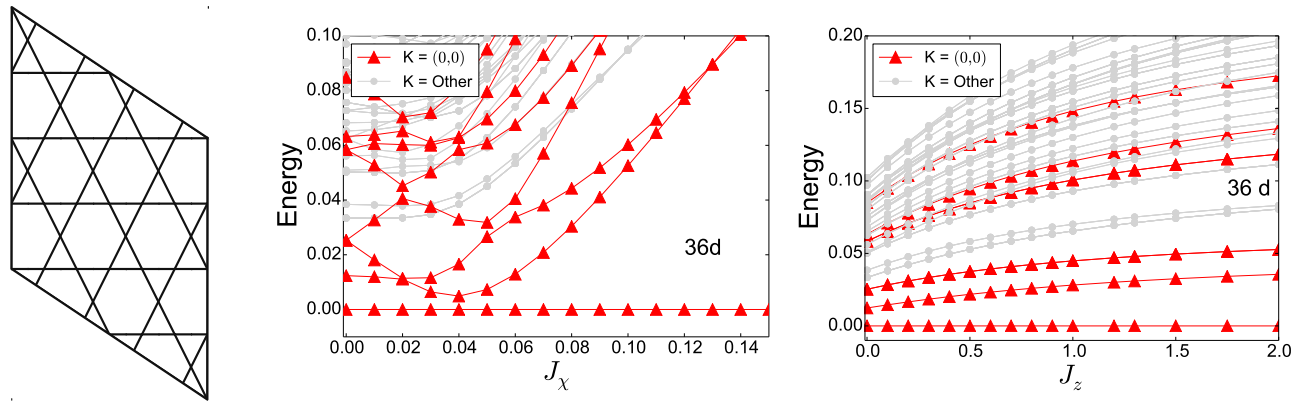

FIG. 9. Left: geometry of the 36d cluster. The energy spectrum as a function of (center) J_χ at $J_z = 0$ and (right) J_z at $J_\chi = 0$ are shown.

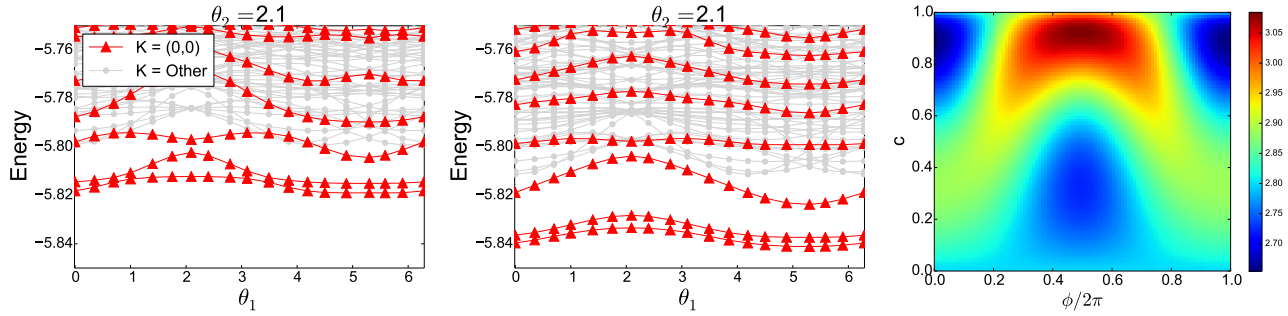

FIG. 10. Spectral flow of low energy wavefunctions for the 36d cluster under twist boundary conditions (varying θ_1) at fixed $\theta_2 = 2.1$ for $J_\chi = 0.01$ (left) and $J_\chi = 0.04$ (center). The former case shows no clear separation of a low energy manifold from the rest of the spectrum, while the latter case shows two topological states. On the right, for $J_\chi = 0.04$, we show the profile of the Renyi entanglement entropy for a topologically non trivial cut as a function of parameters c, ϕ parameterizing the linear combination of the two topological states. Two local minima are detected as seen by the blue regions. The other topologically non trivial cut (not shown) being related by symmetry, has minima at the same location of c, albeit with different ϕ.

Appendix C: Analysis of the 36d cluster

In this appendix we compile all the results for a single cluster, 36d, shown in Fig. 9, and discuss the results together; we find that this cluster is similar to the 48 cluster. This cluster has been studied by several authors [10, 49, 50] primarily in the context of the Heisenberg point of the KAF.

Fig. 9 shows the energy spectrum as a function of J_χ at $J_z = 0$. At $J_\chi = 0$ there are four low energy states (all in $K = (0, 0)$) i.e. two states followed by an exactly degenerate pair. On turning on $J_\chi > 0$, the degenerate pair splits, one of them approaches the ground state becoming quasi-degenerate with the ground state at $J_\chi \approx 0.04$. The first excited state at $J_\chi = 0$ appears to eventually gap out around $J_\chi \approx 0.04$ and beyond.

We checked whether the ground state manifold is clearly separated out from the continuum as a function of twist angles, finding that it is at $J_\chi = 0.04$ but not at $J_\chi = 0.01$ (see Fig. 10). Where the ground state manifold is gapped out, it is sensible to compute the Chern number using the lowest two states within the Non-Abelian formalism. We find that $C = 1$ for the topological manifold, to at least six digits, which corresponds to $C = 1/2$ per state.

We now address the evaluation of the $\mathcal{S}$ matrix. Fig. 10, shows the Renyi entanglement entropy of a topologically non trivial cut as a function of c and ϕ, the parameters that characterize an arbitrary (normalized) linear combination of two eigenstates. Two local minima are observed (see Fig. 10) but they are not orthogonal, the overlap is about 0.147. While the minimum at $c \approx 0.89$ is prominent, the one at $c \approx 0.32$ is located in a relatively flat basin, analogous to the observation in the case of the 42a cluster.

[1] J. S. Helton *et al.*, Phys. Rev. Lett. **98**, 107204 (2007).
[2] P. Mendels *et al.*, Phys. Rev. Lett. **98**, 077204 (2007).
[3] S. Yan, D. A. Huse, and S. R. White, Science **332**, 1173 (2011).
[4] S. Depenbrock, I. P. McCulloch, and U. Schollwöck, Phys. Rev. Lett. **109**, 067201 (2012).
[5] Y. Iqbal, F. Becca, and D. Poilblanc, Phys. Rev. B **84**, 020407 (2011).
[6] G. Evenbly and G. Vidal, Phys. Rev. Lett. **104**, 187203 (2010).

[7] Y. Ran, M. Hermele, P. A. Lee, and X.-G. Wen, Phys. Rev. Lett. **98**, 117205 (2007).
[8] H. C. Jiang, Z. Y. Weng, and D. N. Sheng, Phys. Rev. Lett. **101**, 117203 (2008).
[9] B. K. Clark *et al.*, Phys. Rev. Lett. **111**, 187205 (2013).
[10] A. M. Läuchli, J. Sudan, and E. S. Sørensen, Phys. Rev. B **83**, 212401 (2011).
[11] L. Balents, Nature **464**, 199 (2010).
[12] L. Savary and L. Balents, arXiv:1601.03742 (2016).
[13] M. Norman, arXiv:1604.03048 (2016).
[14] M. P. Zaletel and A. Vishwanath, Phys. Rev. Lett. **114**, 077201 (2015).
[15] S. Sachdev and N. Read, Int. J. Mod. Phys. B **5**, 219 (1991).
[16] E. Fradkin and S. H. Shenker, Phys. Rev. D **19**, 3682 (1979).
[17] R. Moessner and S. L. Sondhi, Phys. Rev. Lett. **86**, 1881 (2001).
[18] A. Y. Kitaev, Annals of Physics **303**, 2 (2003).
[19] M. Freedman, C. Nayak, K. Shtengel, and K. Walker, Ann. Phys. **310**, 428 (2004).
[20] X. G. Wen, F. Wilczek, and A. Zee, Phys. Rev. B **39**, 11413 (1989).
[21] B. Bauer *et al.*, Nat. Commun. **5**, 5137 (2014).
[22] K. Kumar, K. Sun, and E. Fradkin, Phys. Rev. B **92**, 094433 (2015).
[23] D. F. Schroeter, E. Kapit, R. Thomale, and M. Greiter, Phys. Rev. Lett. **99**, 097202 (2007).
[24] R. Thomale, E. Kapit, D. F. Schroeter, and M. Greiter, Phys. Rev. B **80**, 104406 (2009).
[25] A. E. B. Nielsen, J. I. Cirac, and G. Sierra, Phys. Rev. Lett. **108**, 257206 (2012).
[26] A. E. B. Nielsen, G. Sierra, and J. I. Cirac, Nat Commun **4 SP -**, (2013), article.
[27] Y.-C. He, D. N. Sheng, and Y. Chen, Phys. Rev. Lett. **112**, 137202 (2014).
[28] S.-S. Gong, W. Zhu, and D. N. Sheng, Sci. Rep. **4**, 6317 (2014).
[29] W. Zhu, S. S. Gong, and D. N. Sheng, Phys. Rev. B **94**, 035129 (2016).
[30] D. C. Cabra *et al.*, Phys. Rev. B **71**, 144420 (2005).
[31] S. Capponi *et al.*, Phys. Rev. B **88**, 144416 (2013).
[32] S. Nishimoto, N. Shibata, and C. Hotta, Nat Commun **4**, 2287 (2013).
[33] K. Kumar, K. Sun, and E. Fradkin, Phys. Rev. B **90**, 174409 (2014).
[34] V. Kalmeyer and R. B. Laughlin, Phys. Rev. Lett. **59**, 2095 (1987).
[35] X.-G. Wen, Int. J. Mod. Phys. B **4**, 239 (1990).
[36] X. G. Wen, Adv. Phys. **44**, 405 (1995).
[37] E. Fradkin, *Field Theories of Condensed Matter Physics, Secoond Edition*, 2nd ed. (Cambridge University Press, Cambridge, UK, 2013).
[38] E. Witten, Commun. Math. Phys. **121**, 351 (1989).
[39] S. Dong, E. Fradkin, R. G. Leigh, and S. Nowling, JHEP-J. High Energy Phys. **05**, 016 (2008).
[40] P. Di Francesco, P. Mathieu, and D. Sénéchal, *Conformal Field Theory* (Springer-Verlag, Berlin, 1997).
[41] A. Kitaev and J. Preskill, Phys. Rev. Lett. **96**, 110404 (2006).
[42] Y.-F. Wang, Z.-C. Gu, C.-D. Gong, and D. N. Sheng, Phys. Rev. Lett. **107**, 146803 (2011).
[43] R. Yu *et al.*, Phys. Rev. B **84**, 075119 (2011).
[44] H. Shapourian and B. K. Clark, Phys. Rev. B **93**, 035125 (2016).
[45] Y. Zhang *et al.*, Phys. Rev. B **85**, 235151 (2012).
[46] S. Dong, E. Fradkin, R. G. Leigh, and S. Nowling, Journal of High Energy Physics **2008**, 016 (2008).
[47] W. Zhu, D. N. Sheng, and F. D. M. Haldane, Phys. Rev. B **88**, 035122 (2013).
[48] L. Cincio and G. Vidal, Phys. Rev. Lett. **110**, 067208 (2013).
[49] P. W. Leung and V. Elser, Phys. Rev. B **47**, 5459 (1993).
[50] H. Nakano and T. Sakai, Journal of the Physical Society of Japan **80**, 053704 (2011).